

Motile bacteria in a critical fluid mixture

Nick Koumakis,¹ Clémence Devailly,¹ and Wilson C. K. Poon¹

¹*SUPA and School of Physics & Astronomy, The University of Edinburgh,
James Clerk Maxwell Building, Peter Guthrie Tait Road, Edinburgh EH9 3FD, Scotland, UK*

We observed the swimming of *Escherichia coli* bacteria in the vicinity of the critical point in a solution of the non-ionic surfactant $C_{12}E_5$ in buffer solution. In phase contrast microscopy, each swimming cell produces a transient trail behind itself lasting several seconds. Comparing quantitative image analysis and simulations show that these trails are due to local phase re-organisation triggered by differential adsorption. This contrasts with similar trails seen in bacteria swimming in liquid crystals, which are due to shear effects. We show how our trails are controlled and probe the structure and dynamics of critical fluctuations in the fluid medium.

Critical phenomena have fascinated investigators for 150 years [1]. Initially, two paradigmatic instances were studied separately: the loss of magnetism at the Curie temperature, and the disappearance of the vapour-liquid interface at a critical temperature and pressure. The discovery that divergent fluctuations near criticality brought these into the same ‘universality class’ unified statistical and quantum physics, often in surprising ways, e.g., fluctuation-induced interactions [2]. Casimir showed that confining zero-point quantum fluctuations between two surfaces gives rise to an attractive force. Similarly confining critical concentration fluctuations in a fluid mixture gives attractive or repulsive ‘critical Casimir forces’ (CCFs) depending on the differential affinity of the surfaces for the two fluids [3–7]. CCFs between colloids [3, 4] offer new ways to tune their interactions.

Active matter [8] has attracted the attention of diverse investigators in recent years. Self-propelled micro-swimmers, natural or synthetic, are instances of active matter [9]. Their lack of time-reversal symmetry promises new physics [10], and offers novel routes of self assembly [11]. Interestingly, it is possible to utilise critical binary mixtures to generate synthetic self propulsion. If a particle partially coated with gold suspended in such a mixture is illuminated, differential light absorption and therefore local heating gives rise to asymmetric critical fluctuations, which generate a propulsive force [12, 13].

A wall perturbs fluctuations to a distance comparable to the correlation length, $\xi \propto \epsilon^{-\nu}$, where $\epsilon = |(T - T_c)|/T_c$ measures how close the temperature T is to the critical point T_c . At sufficiently small ϵ , $\nu \approx 0.630$ for binary fluids [14]; for larger ϵ , the mean-field exponent $\nu = \frac{1}{2}$ is expected. The characteristic decay time of fluctuations $\tau \propto \epsilon^{-\nu z}$, where the dynamic critical exponent $z = d + x_\eta$ in d dimensions, and $x_\eta \approx 0.068$ [14]. In some systems, ξ/τ can become comparable to typical micro-swimmer speeds ($\gtrsim 10 \mu\text{m s}^{-1}$). In a mixture of the non-ionic surfactant $C_{12}E_5$ and water, $\xi \sim 0.3 \mu\text{m}$ and $\tau \gtrsim 0.01 \text{ s}$ at a readily accessible $\epsilon \sim 10^{-4}$ [15, 16]. New phenomena may therefore arise when active colloids swim in such media.

Here, we show that in a critical $C_{12}E_5$ -water mixture, motile *Escherichia coli*, a model active colloid [17] ‘paint’

a transient pattern of trails reminiscent of the way Jackson Pollock created his iconic canvasses [18]. The trails in our system differ from those seen in bacteria swimming in liquid crystals [19], where shear effects dominate. Our trails relate to the structure and dynamics of critical fluctuations, and corroborate for the first time simulations of passive colloids in critical fluids [20, 21]. Our work demonstrates a fruitful duality in studying active matter in complex media: ‘funnel gate’ arrays [22], gels [23], polymers [24], liquid crystals [19, 25], emulsions [26] and colloidal crystals [27] provide new ways to manipulate micro-swimmers; at the same time, active colloids are micro- and nano-probes of such complex media [19, 24].

We observed smooth-swimming mutants of *E. coli* dispersed in a solution of $C_{12}E_5$ in phosphate motility buffer with added glucose, in which cells remain motile for several hours (see Methods). The solution’s phase diagram, Fig. 1(b), resembles that of $C_{12}E_5$ in water [15, 16], but the critical point is shifted to $c_0 = 1.6\text{wt.}\%$ $C_{12}E_5$ and a lower critical solution temperature (LCST) of $T_c = 27^\circ\text{C}$. We monitored cells swimming at $\gtrsim 6 \mu\text{m s}^{-1}$ in a mixture at c_0 and $3 \times 10^{-4} \lesssim \epsilon \lesssim 3 \times 10^{-3}$ ($\pm 0.1^\circ\text{C}$).

Phase contrast microscopy movies revealed a criss-crossed pattern of $\sim 10 \mu\text{m}$ long phase-bright trails behind swimming cells, Fig. 1(a). In our set up, phase bright corresponds to lower than average refractive index. Since $C_{12}E_5$ has higher index than water [28], our trails should be water rich.

This suggest that *E. coli* surfaces have a higher overall affinity for water than surfactant, which gives rise to a water-rich fluid layer next to the cell whose extent scales as ξ . Near criticality, it extends mesoscopically into the surrounding fluid. As a cell moves, this layer is advected backwards, forming a phase-bright water-rich trail, which then equalises its concentration with the bulk by diffusion. Consistent with this picture, we observed no trails at the same ϵ but a lower $C_{12}E_5$ concentration of $c = 1.0\text{wt.}\% < c_0$, i.e. richer in water than criticality, but did observe trails at $c = 2.0\text{wt.}\%$. Moreover, non-motile bacteria aggregated whenever trails were visible, consistent with attractive CCFs due to preferential water adsorption [7].

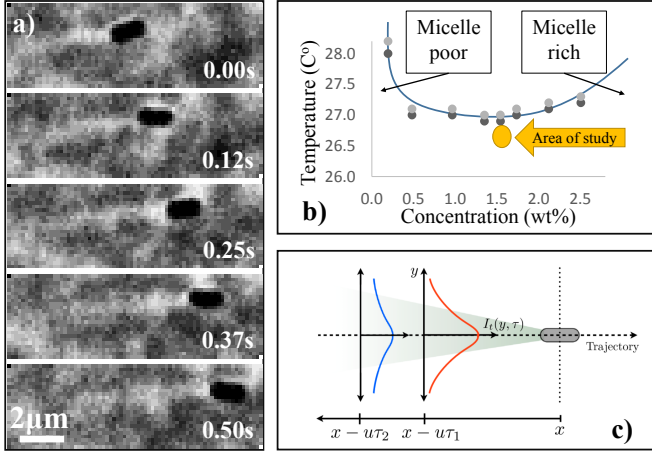


FIG. 1: a) Phase contrast microscopy image snapshots of a single swimming *E. coli* at different times, showing an occurring trail in a phase separating fluid (brighter than the background). The image contrast was increased for clarity. b) Experimental phase diagram of the temperature versus the concentration of C₁₂E₅ in the motility buffer, without bacteria, highlighting the experimental area. Points show the measured upper and lower bounds of the phase separation, while the line is a guide to the eye. c) Schematic of how the trail intensity profiles are extracted from the images.

We model the bacterium as a source moving at velocity $-\mathbf{u}$ and ‘emitting’ water-rich phase at a constant rate Q per unit time. In the co-moving frame, fluid advects past the cell at the origin at velocity \mathbf{u} , and the concentration of water-rich phase, $c(\mathbf{r}, t)$, satisfies mass conservation:

$$\partial_t c + \nabla \cdot \mathbf{j} = Q\delta(\mathbf{r}). \quad (1)$$

Substituting the diffusive and advective fluxes $\mathbf{j}_D = -D\nabla c$ and $\mathbf{j}_A = c\mathbf{u}$ (so that $\mathbf{j} = \mathbf{j}_D + \mathbf{j}_A$) and assuming incompressibility ($\nabla \cdot \mathbf{u} = 0$) gives

$$\partial_t c - D\nabla^2 c + \mathbf{u} \cdot \nabla c = Q\delta(\mathbf{r}), \quad (2)$$

an advection-diffusion equation, which has been used to model pheromone spreading from a moving insect [29]. The neglect of hydrodynamics is plausible *a priori* because of the dipolar or higher order flow field around a bacterium [30], and justified *a posteriori* by fit with experiment.

In the steady state, $\partial_t c = 0$, and let \mathbf{u} be along x . For all times t such that $ut \gg \sqrt{2Dt}$, or $t \gg 2D/u^2$, advection is much faster than diffusion. This requires $x \gg \lambda = 2D/u$. For our $u \gtrsim 6 \mu\text{m s}^{-1}$ and $0.1 \lesssim D \lesssim 1 \mu\text{m}^2 \text{s}^{-1}$ (see later), $\lambda \lesssim 0.3 \mu\text{m}$. In the $x \gg \lambda$ (high Péclet) limit, we neglect diffusion along x , and obtain

$$u\partial_x c = D(\partial_{yy} c + \partial_{zz} c) + Q\delta(\mathbf{r}). \quad (3)$$

For a moving source at $z = h$ above a non-porous wall

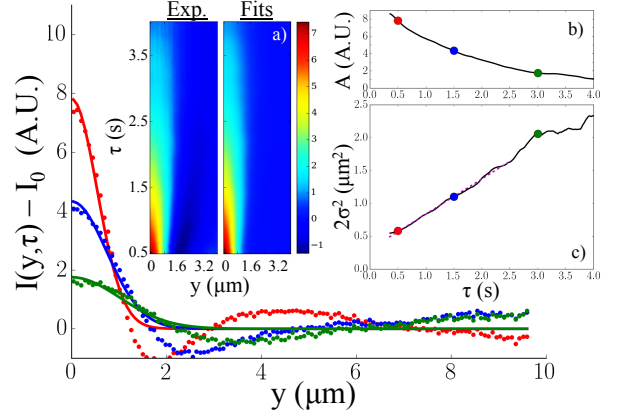


FIG. 2: Main: Figure of three intensity profiles at a near-critical temperature ($\epsilon = 3.3 \cdot 10^{-4}$, or $T_c - T \approx 0.1^\circ\text{C}$) after subtraction of the background for $\tau = 0.5$ (red), 1.5 (blue) and 3.0 s (green). Dots are from analysed data, while solid lines are the Gaussian fits to the data. Inset: a) A contour plot of the intensity profiles as a function of time, for the analysed data and for the fitted curves. The height, b), and variance, c), of the Gaussian fits as a function of time, including a linear fit in c), from which a diffusivity can be extracted (Eq. 7, here $D \approx 0.15 \mu\text{m}^2/\text{s}$).

at $z = 0$, the stationary concentration profile is

$$c(\mathbf{r}) = \sqrt{\frac{Q}{2\pi Dx(\tau)}} \exp\left\{-\frac{uy^2}{4Dx(\tau)}\right\} \sqrt{\frac{Q}{2\pi Dx(\tau)}} \times \left[\exp\left\{-\frac{u(z-h)^2}{4Dx(\tau)}\right\} + \exp\left\{-\frac{u(z+h)^2}{4Dx(\tau)}\right\} \right], \quad (4)$$

with the second z -dependent ‘image’ term enforcing zero flux at $z = 0$. In the lab frame, the distance downstream from the cell in the co-moving frame, x , is parametrised by the time interval τ before the current time t when the cell was at position $x = u\tau$ downstream from its current position, assuming constant u , Fig. 1(c), so that the transverse concentration profile at a fixed z is Gaussian:

$$c(y, \tau) = A(\tau) \exp\left\{-\frac{y^2}{4D\tau}\right\}, \quad (5)$$

If the intensity in our movies, I , is proportional to concentration, then measuring $I_t(y, \tau)$ in individual images, Fig. 1(c), can test Eq. 5. In practice, we average over different frames (i.e., over t) for each of many cells $i = 1$ to $\sim 10^3$. We plot the result with background subtracted, $\langle I(y, \tau) \rangle_{t,i} - I_0$, Fig. 2, including only data from vigorous swimmers, $v > 6 \mu\text{m s}^{-1}$ and for $x = v\tau > 6 \mu\text{m}$, the latter to avoid strong effects from beating flagella. The data can be fitted by Eq. 5:

$$\langle I(y, \tau) \rangle_{t,i} = A(\tau) \exp\left\{-\frac{y^2}{2\sigma(\tau)^2}\right\} + I_0, \quad (6)$$

except that the variance has a constant term:

$$2\sigma^2 = 4D\tau + 2\sigma_0^2, \quad (7)$$

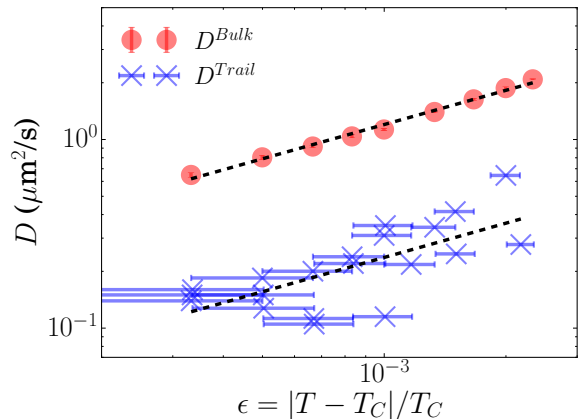


FIG. 3: Diffusivity as a function of normalised distance from criticality, $D(\epsilon)$, measured by fitting trail intensity profiles \times and from differential dynamic microscopy (●). Lines are power-law fits to $D \sim \epsilon^\phi$, which return critical exponents of $\phi = 0.60 \pm 0.15$ and 0.60 ± 0.03 respectively.

with $D \approx 0.15 \mu\text{m}^2 \text{s}^{-1}$ and $\sigma_0 \approx 0.30 \mu\text{m}$, the latter corresponding to a minimum full width of $\lesssim 1 \mu\text{m}$, which is close to the point spread function of our imaging system.

This procedure was repeated at different temperatures to obtain $D^{\text{trail}}(\epsilon)$. Theoretically, we expect $D \sim \epsilon^\phi$, where $\phi = \nu x_D$ with $x_D = d - 2 + x_\eta$ in d dimensions [14], so that in 3D, $\phi \approx 0.63 \times 1.068 = 0.67$ (or, using the mean-field $\nu = \frac{1}{2}$, $\phi = 0.534$). Experimentally, we find $\phi = 0.60 \pm 0.15$ from fitting trail profiles, Fig. 3.

Following Giavazzi et al. [31], we used differential dynamic microscopy (DDM) to measure the diffusivity in the bulk of our mixture (see Methods for details) to give $D^{\text{bulk}}(\epsilon)$, Fig. 3. The data are less noisy than those from fitting trails, and return $\phi = 0.60 \pm 0.03$. In absolute magnitude, however, $D^{\text{bulk}} \approx 5D^{\text{trail}}$. We expect the difference to mainly stem from the trails being observed close to a glass slide. At $\epsilon = 4 \times 10^{-4}$, $D^{\text{bulk}} \approx 1 \mu\text{m}^2 \text{s}^{-1} = k_B T / 6\pi\eta\xi$, from which (neglecting the weak changes of η due to criticality and using $\eta \approx \eta_{\text{H}_2\text{O}} \approx 0.001 \text{ Pa s}$) we estimate $\xi \approx 0.2 \mu\text{m}$ (cf. $\xi \approx 0.3 \mu\text{m}$ at this ϵ from [31]), which is comparable to the radius of the bacterium ($0.4 \mu\text{m}$). Thus, D^{trail} could be significantly retarded by wall hydrodynamics.

To further confirm our claim that the trails are preferentially-adsorbed water-rich layers being advected downstream and explore an alternative mechanism, we simulated the 2D conserved order parameter (COP) Ising model [32]. To model a binary (AB) mixture, the $N \times N$ spins in the COP Ising model are defined to be $s_i = +1$ or -1 if site i is occupied by species A or B. The total energy is $H = \frac{J}{4} \sum_{ij} (1 - s_1 s_2) = \text{constant} - J \sum_{ij} s_i s_j$ summed over nearest neighbours with $J > 0$. We require conservation of $n = N^{-1} \sum_i \sigma_i$, the normalised (signed) difference in numbers of A and B. The critical point is

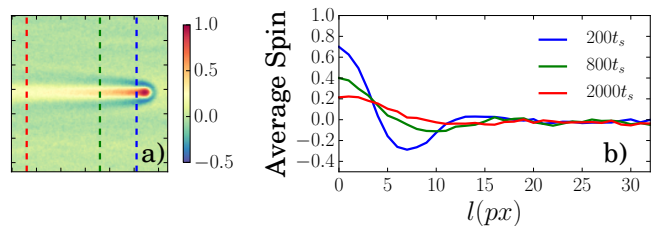


FIG. 4: a) Ising model simulation at $T = 2.8$ ($\epsilon \approx 0.23$) of a trail formed by a Gaussian-shaped energy inclusion (peak value = $5.6k_B T$, standard deviation = 4 pixels (px)) travelling at a speed of $0.05 \text{ px}/t_s$ towards the right. b) Average spin profile from the centre of the inclusion, corresponding to different time scales, as indicated by the color-coded vertical dashed lines in a).

at $T_c \approx 2.27$ in units of J/k_B and $n_c = 0$. We work at n_c , where at $T < T_c$, the system separates into equal amounts of symmetric coexisting A- and B-rich phases, i.e. $n = \pm \Delta n$. In our Monte Carlo (MC) simulations, n -conservation is implemented using Kawasaki (or nearest-neighbour spin exchange) dynamics [32, 33].

For a direct analogue to a bacterium swimming in a critical fluid, we simulated a Gaussian-shaped high-energy region traversing the lattice at $\epsilon \approx 0.23$ and constant speed (see SI) [21]. In the co-moving frame, we see a downstream trail, Fig. 4(a), whose transverse profile $n(y)$ shows a peak that decays oscillatorily, Fig. 4(b), as in experiments, Fig. 2, although the oscillations in the latter are partly artefacts of phase-contrast imaging [34].

The high shear rate near rotating flagella, $\dot{\gamma} \sim 10^4 \text{ s}^{-1}$ [24], can also generate a phase-bright trail in our system. If $\dot{\gamma}^{-1} \lesssim \tau$, the decay time of the fluctuations, we may expect the flow to homogenise the fluctuations [35], reducing ξ and therefore scattered light. The advection of a homogenised region downstream generates a phase-bright trail. Indeed, shear melting by flagella is responsible for bacterial trails in liquid crystals [19].

To explore this possibility, we simulated the evolution of two kinds of stripes embedded in a near-critical COP Ising lattice ($\epsilon \approx 0.035, n = 0$) (see Methods). To mimic a shear-homogenised region, we used a stripe initially at a much higher temperature ($\epsilon \approx 0.76$), evidenced by the finer-scale fluctuations in the stripe compared to the bulk, Fig. 5(a). Visually, this region becomes barely distinguishable from the bulk within $\tau_R^{\text{shear}} \sim 500t_s$, where t_s is the MC time step. Plots of the energy profile of the stripe, $H(l)$, at increasing times verify this observation.

To mimic a water-rich trail, we prepared a stripe of positive spins at $\epsilon \approx 0.19$. Visual inspection and the $H(l)$ plot show that relaxation now takes $\sim 10^5 t_s \gtrsim 10^2 \tau_R^{\text{shear}}$. This is because a homogenised trail has the bulk concentration ($n = 0$), but a stripe of up spins has a different concentration ($n = 1$). Relaxation of the latter requires long-range transport subject to conserved (Kawasaki) dy-

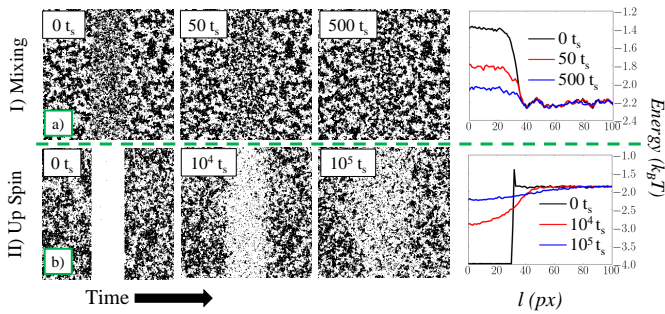


FIG. 5: Simulations of 64-site wide 'trails' with different initial conditions embedded in a COP Ising lattice at $T_{\text{Bulk}} = 2.7$ ($\epsilon \approx 0.19$). Snapshots are shown at time $t = 0$ and two other times in units of Monte Carlo time step, t_s , and plots of the average energy as a function of the distance from the centre of the profile (l). a) A stripe initially at a higher temperature, $T = 4$ ($\epsilon \approx 0.76$). b) A stripe initially with all up spins at $T = 2.7$.

namics. Thus, if shear effects are present in our system, they will be masked by much slower differential adsorption effects.

The COP Ising model belongs to the same universality class as binary fluids with identical static critical exponents. Nevertheless, we do not attempt a more quantitative comparison between simulations and experiments, since dynamical critical phenomena and exponents are model dependent [36, 37], while also sensitive to details, e.g. the presence or absence of hydrodynamics. Thus, we would not expect the diffusivity exponents to be the same, although qualitative conclusions such as those we have reached above should remain valid.

We have observed *E. coli* swimming in a critical mixture of water and the surfactant C_5E_{12} . They leave transient trails. That these trails are bright in phase contrast imaging together with analytic modelling and simulations suggest strongly that they are due to a preferentially-adsorbed water-rich layer on cell surfaces of mesoscopic extent due to proximity to criticality. This is advected downstream as cells swims. Similar physics – preferential adsorption near criticality, underlies CCFs between colloids in critical fluid mixtures. By fitting the transverse intensity profile of our trails, we obtained a diffusivity dynamical critical exponent that scales with the best theoretical estimates to date, thus offering the first example of using active matter to probe critical phenomena.

METHODS

We cultured a ΔcheY (non-tumbling) mutant of strain AB1157 in Luria Broth (LB) agar plates, then transferred to 10ml of liquid LB to be incubated at 30°C overnight. Then $350 \mu\text{L}$ of this culture was transferred into 35mL

of Terrific Broth (TB) to grow for 4h, reaching mid-exponential phase. Cells were then washed 3 times in a motility buffer (MB: $6.2 \text{ mM K}_2\text{HPO}_4$ (Sigma-Aldrich), $3.8 \text{ mM KH}_2\text{PO}_4$ (Fisher Chemical) and 0.1mM EDTA (Sigma Aldrich)) using a filter unit and $0.45\mu\text{m}$ filter paper. We then transfer the bacteria into our critical fluid. Our final critical fluid consists of a mixture of 1.6 w/w\% pentaethylene glycol monododecyl ether, $C_{12}E_5$, (Sigma Aldrich), a non-ionic surfactant, the Motility Buffer (MB) and 1.5 mM glucose. The glucose promotes stable swimming for several hours [17], while the concentration of $C_{12}E_5$ is non-harmful to *E. coli* swimming. The final bacterial suspension, having an optical density (OD) between 0.05 and 0.1 , was loaded into $50\mu\text{m} \times 0.5\text{mm}$ rectangular capillaries (CM Scientific).

We used a lower critical solution temperature (LCST) critical mixture. This critical mixture was chosen because of its large microscopic correlation length and flat phase boundary near criticality, the latter giving a large window for observing critical fluctuations [16]. The solution was stored away from light. The precise phase boundary varied between experiments due to sample degradation by dissolved CO_2 and photodissociation (minimised by storage in the dark) as well as external temperature variations. Therefore, T_c was determined in each experiment separately, by warming a sample up from the single-phase to the two-phase region through the critical point. The trail measurements were then taken immediately using a sample in a fresh capillary to avoid any hysteresis effects from improper remixing [38].

Using phase contrast microscopy (Nikon $20\times \text{ph1}$ and $60\times \text{ELWD ph3}$ objectives) near a glass surface and a 16-bit high-sensitivity camera (Orca Flash, Hamamatsu), we imaged bacteria and their trails. An INSTEC temperature stage (mK1000) kept the sample temperature stable to $\pm 0.1^\circ\text{C}$. The samples were taken to just below T_c , and then measurements at different ϵ were carried out by successively decreasing the temperature. Ten 40s movies at 100 frames per second were taken at each temperature after stabilising for 5 min.

We extracted the diffusion coefficient D of the density fluctuations using differential dynamic microscopy (DDM) following a published protocol [39]. Movies of the binary mixture without bacteria at different temperatures were taken ($60\times \text{ELWD ph3}$ Nikon objective, 40s at 100 frames per second, 512×512 and 4×4 binning). This gave access to a wave vector range of $0.05 \leq q \leq 6.6 \mu\text{m}^{-1}$. The extracted differential intermediate scattering functions [39] exhibited single exponential decay, which we fitted with $A(q)(1 - e^{-Dq^2t}) + B(q)$, where t is the delay time between two frames. $A(q)$ is determined by the structure factor and form factor of the sample, and $B(q)$ measured camera noise. We obtained a value of D for each available q and averaged over $0.5 \leq q \leq 2.4 \mu\text{m}^{-1}$, the region in which reliable correlation functions could be obtained.

The conserved order parameter Ising model and its mapping onto a binary mixture has been described in the main text. At each step of our Monte Carlo simulation, we chose a random site and one of its neighbours and calculated the energy change ΔE for exchanging the two spins. We used the heat-Bath algorithm [32], i.e. a spin exchange probability of $p = (1 + e^{\Delta E/T})^{-1}$. We define t_s as the time when spin exchange attempts = number of cells in the system. Simulations were performed over for of $T = 2.7$ and 2.8 ($T_c \approx 2.27$, $\epsilon = 0.19$, 0.23) [32] on 1050×1050 and 540×540 cell systems.

Two types of simulations were performed. Initially (fig.4), in order to mimic a swimming bacterium, we allowed our Ising model simulation to progress at $T = 2.8$ ($\epsilon \approx 0.23$), with a Gaussian-shaped energy inclusion (peak value = $5.6k_B T$, standard deviation = 4 pixels (px)) travelling at a speed of 0.05 px/ t_s . We extracted the average spin when centred around the energy inclusion, after reaching a steady state. To distinguish the origin of the trail between phase separation and shear mixing a second simulation was performed (fig.5), where a 'trail' was imposed and let to equilibrate. For local phase separation, we allowed the simulation to equilibrate at $T = 2.7$ ($\epsilon \approx 0.19$) and subsequently applied a positive spin trail. In the case of mixing, we constructed initial conditions by imposing a projected 1D spatial variation of a high temperature and simulated until a steady state was reached. The spatial variation for the temperature or spin profile was either a step function with a diameter of 64 sites. A waiting time of $t = 100000t_s$ was found to be sufficient for reaching a steady state in all cases. The new profile was then allowed to equilibrate without external control and the the relaxation dynamics were qualitatively compared to the experiments. We typically averaged results from > 10 runs for all the simulations.

Acknowledgements: We thank J. Arlt, A. Brown, B. Guy, V. Martinez and T. Vissers for discussions. NK was part-funded by the EU (H2020-MSCA-IF-2014, ActiDoC No. 654688). All received funding from UK EPSRC (EP/J007404/1) and ERC (Advanced Grant ERC-2013-AdG 340877-PHYSAP).

-
- [1] C. Domb, *The Critical Point: A Historical Introduction To The Modern Theory Of Critical Phenomena* (CRC Press, 1996).
- [2] M. Kardar and R. Golestanian, *Rev. Mod. Phys.* **71**, 1233 (1999).
- [3] C. Hertlein, L. Helden, A. Gambassi, S. Dietrich, and C. Bechinger, *Nature* **451**(7175), 172 (2008).
- [4] A. Gambassi, A. Maciolek, C. Hertlein, U. Nellen, L. Helden, C. Bechinger, and S. Dietrich, *Phys. Rev. E* **80**, 061143 (Dec 2009).
- [5] A. Gambassi, *J. Phys.: Conf. Ser.* **161**(1), 012037 (2009).
- [6] U. Nellen, L. Helden, and C. Bechinger, *EPL* **88**(2), 26001 (2009).
- [7] O. A. Vasilyev, *Physical Review E* **90**(1), 012138 (2014).
- [8] S. Ramaswamy, *Ann. Rev. Condens. Matter Phys.* **1**(1), 323 (2010).
- [9] W. C. K. Poon, in C. Bechinger, F. Sciortino, and P. Zifferl, eds., *Physics of Complex Colloids* (IOS Press, Amsterdam, 2013), pp. 317–386.
- [10] M. E. Cates, *Rep. Prog. Phys.* **75**, 042601 (2012).
- [11] J. Stenhammar, R. Wittkowski, D. Marenduzzo, and M. E. Cates, *Sci. Adv.* **2**(4) (2016).
- [12] I. Buttinoni, G. Volpe, F. Kümmerl, G. Volpe, and C. Bechinger, *J. Phys.: Condens. Matter* **24**(28), 284129 (2012).
- [13] I. Buttinoni, J. Bialké, F. Kümmerl, H. Löwen, C. Bechinger, and T. Speck, *Phys. Rev. Lett.* **110**, 238301 (Jun 2013).
- [14] S. Roy, S. Dietrich, and F. Höfling, *J. Chem. Phys.* **145**(13), 134505 (2016).
- [15] K. Hamano, T. Sato, T. Koyama, and N. Kuwahara, *Phys. Rev. Lett.* **55**(14), 1472 (1985).
- [16] K. Hamano, K. Fukuhara, N. Kuwahara, E. Ducros, M. Benseddik, J. Rouch, and P. Tartaglia, *Phys. Rev. E* **52**(1), 746 (1995).
- [17] J. Schwarz-Linek, J. Arlt, A. Jepsen, A. Dawson, T. Vissers, D. Miroli, T. Pilizota, V. A. Martinez, and W. C. K. Poon, *Colloids Surf. B* **137**, 2 (2016).
- [18] L. Emmerling, *Pollock* (Taschen, 2016).
- [19] S. Zhou, A. Sokolov, O. D. Lavrentovich, and I. S. Aranson, *Proc. Natl. Acad. Sci. (USA)* **111**(4), 1265 (2014).
- [20] A. Furukawa, A. Gambassi, S. Dietrich, and H. Tanaka, *Phys. Rev. Lett.* **111**, 055701 (Jul 2013).
- [21] V. Démery and D. S. Dean, *Phys. Rev. Lett.* **104**, 080601 (Feb 2010).
- [22] P. Galajda, J. Keymer, P. Chaikin, and R. Austin, *J. Bact.* **189**, 8704 (2007).
- [23] O. A. Croze, G. P. Ferguson, M. E. Cates, and W. C. K. Poon, *Biophys. J.* **101**, 525 (2011).
- [24] V. A. Martinez, J. Schwarz-Linek, M. Reufer, L. G. Wilson, A. N. Morozov, and W. C. K. Poon, *Proc. Natl. Acad. Sci. (USA)* **111**(50), 17771 (2014).
- [25] P. C. Mushenheim, R. R. Trivedi, H. H. Tuson, D. B. Weibel, and N. L. Abbott, *Soft Matter* **10**, 88 (2014).
- [26] I. D. Vladescu, E. J. Marsden, J. Schwarz-Linek, V. A. Martinez, J. Arlt, A. N. Morozov, D. Marenduzzo, M. E. Cates, and W. C. K. Poon, *Phys. Rev. Lett.* **113**, 268101 (Dec 2014).
- [27] A. T. Brown, I. D. Vladescu, A. Dawson, T. Vissers, J. Schwarz-Linek, J. S. Lintuvuori, and W. C. K. Poon, *Soft Matter* **12**(1), 131 (2016).
- [28] B.-H. Chen, C. A. Miller, J. M. Walsh, P. B. Warren, J. N. Ruddock, P. R. Garrett, F. Argoul, and C. Leger, *Langmuir* **16**(12), 5276 (2000).
- [29] A. Okubo and S. A. Levin, *Diffusion and Ecological Problems: Modern Perspectives* (Springer, New York, 2001).
- [30] K. Drescher, R. E. Goldstein, N. Michel, M. Polin, and I. Tuval, *Phys. Rev. Lett.* **105**, 168101 (2010).
- [31] F. Giavazzi, A. Fornasieri, A. Vailati, and R. Cerbino, *The European Physical Journal E* **39**(10), 103 (2016).
- [32] M. E. J. Newman and G. T. Barkema, *Monte Carlo Methods in Statistical Physics* (Oxford University Press: New York, USA, 1999).
- [33] K. Kawasaki, *Phys. Rev.* **145**, 224 (May 1966).
- [34] M. S. Elliot and W. C. Poon, *Adv. Colloid Interface Sci.*

-
- 92**(1), 133 (2001).
- [35] A. Onuki, *J. Phys.: Condens. Matter* **9**(29), 6119 (1997).
 - [36] P. C. Hohenberg and B. I. Halperin, *Rev. Mod. Phys.* **49**, 435 (1977).
 - [37] R. Folk and G. Moser, *J. Phys. A: Math. Gen.* **39**(24), R207 (2006).
 - [38] I. A. Martinez, C. Devailly, A. Petrosyan, and S. Ciliberto, *Entropy* **19**(77) (2017).
 - [39] F. Giavazzi, A. Fornasieri, A. Vailati, and R. Cerbino, *Eur. Phys. J. E* **39**(10), 103 (Oct 2016).